Chemical Engineering Journal 258 (2014) 374–385

Contents lists available at ScienceDirect

Chemical Engineering Journal

journal homepage: www.elsevier.com/locate/cej

Asymptotic model for deep bed filtration

Zhenjiang You [a,*], Yuri Osipov [b], Pavel Bedrikovetsky [a], Liudmila Kuzmina [c]

[a] Australian School of Petroleum, The University of Adelaide, SA 5005, Australia
[b] Moscow State University of Civil Engineering, 26 Yaroslavskoe shosse, Moscow 129337, Russia
[c] National Research University Higher School of Economics, 20 Myasnitskaya Ulitsa, Moscow 101000, Russia

HIGHLIGHTS

- Analytical asymptotic model for non-linear deep bed filtration.
- Explicit formulae to treat long-term laboratory data on colloidal suspension flow.
- Data treatment from the period 5–10 times longer than that used by classical method.
- Fewer laboratory tests required to adjust micro scale population balance model.
- Accuracy–uncertainty criteria of colloidal flow laboratory and asymptotic modelling.

GRAPHICAL ABSTRACT

Evolution of pore size distribution for size exclusion deep bed filtration in porous media.

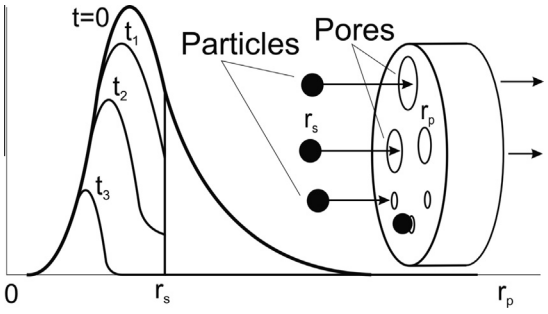

ARTICLE INFO

Article history:
Received 13 May 2014
Received in revised form 8 July 2014
Accepted 10 July 2014
Available online 23 July 2014

Keywords:
Deep bed filtration
Colloid
Porous media
Size exclusion
Pore size distribution
Stochastic model

ABSTRACT

Asymptotic solution for non-linear stage of colloidal suspension flow in porous media is developed. The expansion is performed behind the concentration front; the zero order approximation coincides with the short-time solution of the linearised system. Using the first order approximation allows significantly enhancing the validity time period for the analytical model if compared with the linearised solution, allowing using the long-term experimental breakthrough concentration history for the model adjustment. Laboratory injection tests for three size colloids are performed. The asymptotic solution is used to tune the model parameters from the breakthrough histories of two size particles; good quality of matching is observed. The breakthrough concentration history for the third size particles is compared with the prediction by the adjusted model; good quality prediction is observed. The above serves for validation of the asymptotic method for the model tuning and prediction of non-linear colloidal suspension flow in porous media.

1. Introduction

Colloidal suspension flow in porous media with particle capture is essential for numerous chemical, environmental and petroleum technologies. It takes place in industrial filtering, size exclusion chromatography, water production by artesian wells, industrial waste disposal, aquifer remediation, contamination of aquifers by viruses and bacteria, low quality water injection in oilfields, and fines migration in low consolidate and high-clay-content oil reservoirs [1–11].

Planning and design of the above chemical engineering and petroleum technologies are based on mathematical modelling.

Deep bed filtration of colloidal suspensions in porous media is described by the equation of mass balance of suspended and retained particles and the retention rate equation [12–14]:

* Corresponding author. Fax: +61 8 8303 4345.
E-mail address: zyou@asp.adelaide.edu.au (Z. You).

http://dx.doi.org/10.1016/j.cej.2014.07.051
1385-8947/

Nomenclature

a	reciprocal of the front speed
C	suspended particle concentration distribution by sizes, L^{-4}
C_v	variance coefficient
c	total suspended particle concentration, L^{-3}
D	accuracy of the asymptotic model
E	normalised least square deviation of the model from the measured data
f_a	accessible fractional flow function
H	pore concentration distribution by sizes, L^{-3}
h	total pore concentration (density), L^{-2}
j	jamming ratio
k	permeability, L^2
k_1	conductance in a single pore, L^4
l	inter-chamber distance, L
p_a	particle attachment probability
r_p	radius of a pore, L
r_s	radius of a particle, L
S	dimensionless captured particle concentration
t	time, T or dimensionless
t_f	total injection time
U	Darcy velocity, LT^{-1}
u	combined standard uncertainties
x	linear coordinate, L or dimensionless
y	independent variable in the differential-integral system

Greek letters

δ	Dirac delta function
δ_C	relative combined standard uncertainties for suspended concentration
δ_S	relative combined standard uncertainties for retained concentration
ζ_b	zeta potential for glass beads, $ML^2\,T^{-3}\,I^{-1}$
Λ	dimensionless filtration coefficient
λ	filtration coefficient, L^{-1}
ν	flux reduction factor in a single pore
σ	total concentration of captured particles, L^{-3}
ϕ	porosity
ϕ_a	accessible porosity
Σ	captured particle concentration distribution by sizes, L^{-4}
ψ_s	surface potential for particles, $ML^2\,T^{-3}\,I^{-1}$

Subscripts

a	accessible
C	suspended concentration
S	retained concentration
p	pore
0	initial value
0,1,2	the zero, first and second order of asymptotic solution

Superscripts

0	boundary value at the inlet
L	boundary value at the outlet

$$\frac{\partial}{\partial t}(\phi s c+\sigma)+U\frac{\partial}{\partial x}(c f_a)=0,\ f_a=1 \tag{1}$$

$$\frac{\partial \sigma}{\partial t}=\lambda(\sigma)Uc \tag{2}$$

where $\lambda(\sigma)$ is the filtration coefficient and s is the accessibility factor that is equal to the ratio between the porosity accessible to particles and the overall rock porosity. The fractional flow function f_a corresponds to the fraction of the overall flux moving via the accessible pores [15,16].

At low retained concentration σ, the filtration coefficient becomes constant $\lambda(0)$ and the system becomes linear, allowing for exact solution for clean bed injection with constant concentration c^0:

$$c(x,t)=\begin{cases}\exp\left(-\frac{\lambda}{f_a}x\right), & t>a\\ 0, & t<ax\end{cases},\ \sigma(x,t)=\begin{cases}\lambda(t-ax)\exp\left(-\frac{\lambda}{f_a}x\right), & t>ax\\ 0, & t<ax\end{cases},\ a=\frac{\phi s}{f_a} \tag{3}$$

More complex solutions for deep bed filtration accounting for diffusion are presented by van Genuchten and Alves [17], Ziskind et al. [18] and Guerrero et al. [19,20].

Population balance models for colloidal suspension flows in porous media include particle size distributions of suspended and retained concentrations and pore throat size distribution [21–24]. The models describe the distribution changes due to different attachment and straining rates of different size particles in different size pores.

Other micro scale models include stochastic trajectory analysis [25,26], random walk master equation [27–32] and direct pore scale simulation [14,33].

The model adjustment from the laboratory data is necessary for reliable process prediction by the mathematical modelling. The adjustment of deep bed filtration models is performed by solving the inverse problems [34,35] or by least square tuning of the model parameters [36]. Presently the tuning is performed using the analytical solution for the linearised population balance model (3), where the breakthrough concentration values $c(1,t_{br})$ for particles with different radii r_s are used to determine the filtration coefficient $\lambda(r_s)$ [37]. So, only one tuning constant is retrieved per one size of the injected particles, i.e. one measurement (3) provides with just a single constant for tuning of the population balance model.

It significantly limits the experimental information necessary for the population balance model adjustment due to limited number of particle sizes available on the market. The amount of experimental information can be significantly increased by using the suspended concentration histories long after the breakthrough moment, but the expressions (3) are valid during short after-the-breakthrough periods.

Moreover, the accurate determination of suspension concentration in the breakthrough time cannot be done from one measurement, so the average from the "neighbouring" points is taken. Yet, the retention concentration grows after the breakthrough moment; it is not accounted for in the solution (3) and decreases the accuracy of $c(L,L/U)$ calculation. Despite the method (3) is widely spread, the time period after the breakthrough where the method is valid has never been estimated.

In the present work, the asymptotic model for non-linear deep bed filtration processes is developed. The zero order approximation coincides with the known solution of the linearised system (3). The first order approximation allows prolonging significantly the time period, where the breakthrough concentration can be

used for the model adjustment, allowing increasing the number of independent constants to adjust the population balance model by three. The second order approximation allows determining the validity time interval for the first order approximation.

The laboratory deep bed filtration is performed for colloids of three different sizes. The analytical method allows the population balance model adjustment from two-particle-size filtration and predictive modelling for a third size particle. It was found out that under the common accuracy of the colloidal flow test, the first order approximation model can use the breakthrough concentration during 110 pore volumes injected (PVI) while the solution (3) is valid for 10 PVI. Good match of the laboratory data for two size particles and good agreement between predictive modelling and experimental data for third size particles validate the proposed method for the population balance model tuning based on the asymptotic solution.

The paper is organised as follows. The population balance equations and their upscaling are briefly presented in Section 2. Section 3 derives the asymptotic solution for one-dimensional suspension injection at large scale; the detailed derivations are given in Supplementary Information. Downscaling of the asymptotic solution along with the derivation of pore throat size distribution during size exclusion is given in Section 4. Section 5 describes the laboratory tests on one-dimensional suspension injection. The asymptotic model is adjusted by the experimental data in Section 6, where the method validity is also analysed from the point of view of uncertainties and errors in measurements and modelling. The paper is concluded by discussions of the validity of asymptotic method for adjustment of non-linear population balance model for colloidal suspension flow in porous media.

2. Stochastic model for colloidal suspension transport in porous media

A simplified geometric structure of the parallel bundles of size distributed cylindrical capillary intercalated by the mixing chambers is assumed for the modelling of suspension and colloids in porous media (Fig. 1). Complete mixing occurs in the chambers. A spherical particle larger than the capillary cross sections is irreversibly captured at the entrance of this capillary at the chamber exit, while the smaller spheres continue motion in thicker capillary.

The total concentrations of suspended particles, retained particles and pores (c, σ and h, respectively) are obtained by averaging of the corresponding size distributed concentrations:

$$c(x,t)=\int_0^\infty C(r_s,x,t)dr_s \tag{4}$$

$$\sigma(x,t)=\int_0^\infty \Sigma(r_s,x,t)dr_s \tag{5}$$

$$h(x,t)=\int_0^\infty H(r_p,x,t)dr_p \tag{6}$$

Here the surface pore concentration H is defined by the number of pores crossing the unity cross section area and is equal to volumetric concentration times the inter-chamber distance l.

Flow of size distributed particles in porous media with the varying size pores is described by the system of three equations: the population balance equation for suspended and retained particles, the kinetic equation for particle retention and the equation for pore plugging (see [24] for detailed derivations):

$$\frac{\partial}{\partial t}\{\phi_a[H,r_s]C(r_s,x,t)+\Sigma(r_s,x,t)\}+U\frac{\partial}{\partial x}\{C(r_s,x,t)f_a[H,r_s]\}=0 \tag{7}$$

$$\frac{\partial\Sigma(r_s,x,t)}{\partial t}=\frac{UC(r_s,x,t)f_a[H,r_s]}{lk[H]}\int_0^\infty[1-v(j)+v(j)p_a]k_1(r_p)H(r_p,x,t)dr_p \tag{8}$$

$$\frac{\partial H(r_p,x,t)}{\partial t}=-\frac{k_1(r_p)}{k}UH(r_p,x,t)\int_0^\infty[1-v(j)+v(j)p_a]C(r_s,x,t)f_a[H,r_s]dr_s \tag{9}$$

Here p_a is the particle attachment probability, the flux reduction factor in a single pore v is a function of jamming ratio $j=r_s/r_p$ and l is the inter-chamber distance:

$$v(j)=\begin{cases}(1-j)^2(1+2j-j^2), & j<1\\ 0, & j\geqslant 1\end{cases},\qquad l=l_0(1-f_a)^\beta \tag{10}$$

The accessible and overall porosity are obtained by the pore cross section averaging:

$$\phi_a[H,r_s]=\int_{r_s}^\infty \pi r_p^2H(r_p,x,t)dr_p,\qquad \phi[H]=\int_0^\infty \pi r_p^2H(r_p,x,t)dr_p \tag{11}$$

The fractional function for accessible flow is obtained by the averaging of the flux over all pores:

$$f_a[H,r_s]=\frac{1}{k}\int_0^\infty v(j)k_1(r_p)H(r_p,x,t)dr_p \tag{12}$$

where the conductivity of a single pore and the overall rock permeability are

$$k_1(r_p)=\pi r_p^4/8,\qquad k[H]=\int_0^\infty k_1(r_p)H(r_p,x,t)dr_p \tag{13}$$

Introduction of accessible and inaccessible flows, f_a and $1-f_a$, makes the suspension transport in porous media analogous to two-phase immiscible flow, where ϕ_a/ϕ and $(\phi-\phi_a)/\phi$ are phase saturations (see [1] for detailed derivations).

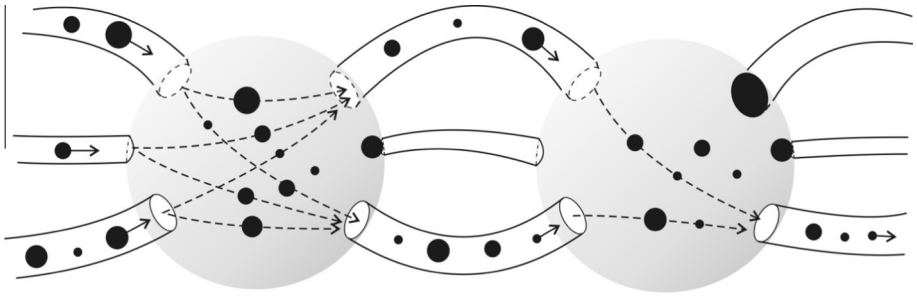

Fig. 1. Geometric model of porous media: parallel capillary bundles alternated by mixing chambers.

Under the condition of complete pore plugging, the sum of volumetric concentrations of vacant pores and retained particles is constant, i.e. $h/l + \sigma = h_0/l + \sigma_0$.

In the particular case of mono-sized suspension flow

$$C(r_s, x, t) = c(x, t)\delta(r_s - r_0) \tag{14}$$

system (7–9) allows for exact solution

$$H(r_p, x, t) = H(r_p, y(h)) = H_0(r_p)e^{-[1-v(j)+v(j)p_a]k_1(r_p)y(h)};$$
$$y = 0 : H = H_0(r_p) \tag{15}$$

where the auxiliary function $y(h)$ is implicitly determined by

$$h(y) = \int_0^\infty H_0(r_p)e^{-[1-v(j)+v(j)p_a]k_1(r_p)y}dr_p; \quad y = 0 : h = h_0 \tag{16}$$

Substituting (14–16) into system (7–9) and integrating in r_s from zero to infinity yields:

$$\frac{\partial}{\partial t}(\phi_a(\sigma)c + \sigma) + U\frac{\partial}{\partial x}(cf_a(\sigma)) = 0 \tag{17}$$

$$\frac{\partial \sigma}{\partial t} = \lambda(\sigma)Uc \tag{18}$$

where the effective material functions of the phenomenological model (17, 18) – accessible porosity $\phi_a(\sigma)$, fractional flow $f_a(\sigma)$ and filtration coefficient $\lambda(\sigma)$ – are calculated from the micro scale model (8, 11, 12) as

$$\phi_a(\sigma) = \int_{r_0}^\infty \pi r_p^2 H_0(r_p)e^{-[1-v(j)+v(j)p_a]k_1(r_p)y(h_0-l\sigma)}dr_p \tag{19}$$

$$f_a(\sigma) = \frac{1}{k(\sigma)}\int_0^\infty v(j)k_1(r_p)H_0(r_p)e^{-[1-v(j)+v(j)p_a]k_1(r_p)y(h_0-l\sigma)}dr_p \tag{20}$$

$$\lambda(\sigma) = \frac{1}{lk(\sigma)}f_a(\sigma)\int_0^\infty [1 - v(j) + v(j)p_a]k_1(r_p)H_0(r_p)e^{-[1-v(j)+v(j)p_a]k_1(r_p)y(h_0-l\sigma)}dr_p \tag{21}$$

where $k(\sigma) = \int_0^\infty k_1(r_p)H_0(r_p)e^{-[1-v(j)+v(j)p_a]k_1(r_p)y(h_0-l\sigma)}dr_p$.

For mono-sized suspension transport, the unknowns for the system (17, 18) are the averaged particle concentrations c and σ and size distributed concentration of pores H, i.e. the system is defined at the pore scale. However, system (17, 18) depends on all the averaged concentrations, i.e. the transformation (15, 16) along with averaging realise the exact upscaling.

For size exclusion particle capture, the particle attachment probability $p_a = 0$; therefore, the filtration coefficient becomes $\lambda(\sigma) = \frac{1}{l}f_a(\sigma)[1 - f_a(\sigma)]$ (see [38]).

The procedure (15, 16) allows for inversion, i.e. the distributed pore concentration $H(r_p, x, t)$ can be calculated from each solution of the upscale system (17, 18).

Introduction of the dimensionless parameters $x \to x/L$, $t \to Ut/L\phi_0$, $C = c/c^0$, $S = \sigma/c^0\phi_0$, $\Lambda = \lambda(\sigma)L$ and $s = \phi_a/\phi_0$ leads to the following dimensionless form of the governing Eqs. (17, 18):

$$\frac{\partial}{\partial t}(s(S)C + S) + \frac{\partial}{\partial x}(Cf_a(S)) = 0 \tag{22}$$

$$\frac{\partial S}{\partial t} = \Lambda(S)C \tag{23}$$

Constant concentration injection into clean porous media corresponds to the following initial and boundary conditions:

$$t = 0 : C = S = 0 \tag{24}$$

$$x = 0 : C = 1 \tag{25}$$

The system (22, 23) contains both time and special derivatives of suspended concentration, so both initial and boundary conditions are posed for C. The system contains only time derivative for retained concentration, so only initial condition for S is posed. The boundary $x = 0$ coincides with characteristic line for Eq. (23). Therefore, the retained concentration at the inlet boundary $S(0,t)$ can be found by substituting the boundary condition $C = 1$ into Eq. (23) and separating variables in the obtained ordinary differential equation

$$\int_0^{S(0,t)} \frac{du}{\Lambda(u)} = t$$

i.e., (22–25) is a Goursat problem [39].

The characteristic form of the system (22, 23) shows that ahead of the front (for $x > t/a$, where $a = s(0)/f_a(0)$ is the reciprocal of the front speed), the suspended and retained concentration is equal to zero. As it follows from (23), the retained concentration is a continuous function (see [1] for proof). Therefore, the retained concentration along the front is equal to zero.

The characteristic lines of the system (22, 23) with velocity f_a/s start at the inlet boundary $x = 0$ and completely cover the domain $x > 0$, $t - ax > 0$ (see Eq. (A2)). So, boundary condition (25) and the value $S = 0$ on the concentration front $t = ax$ provide with the unique solution.

Characteristic line passing point (0,0) in the (x,t) plane coincides with the concentration front. Therefore, the suspended concentration along the front can be also found from the condition $S = 0$; the expression is derived in Supplementary Information.

Suspended and retained concentrations are positive behind the concentration front. The corresponding asymptotic solution of the problem (22–25) is derived in the next section.

3. Asymptotic solution

Let us consider particle concentrations behind the front. The suspension concentration $C(1,t)$ is measured at the core effluent after the breakthrough, i.e. for $x = 1$, $t > a$. This half-interval $(1, [a, \infty])$ in plane (x,t) belongs to the domain behind the concentration front $t - ax = t_0 > 0$ (Fig. 2). The period from the moment of passing of the concentration front up to the current moment $t_0 = t - ax$ is assumed to be a small parameter in the domain behind the front. Therefore, the asymptotic solution of the system (22, 23) subject to the boundary condition (25) and zero value of S on the front is presented in the following series form

$$C(x, t) = c_0(x) + (t - ax)c_1(x) + (t - ax)^2c_2(x) + \dots \tag{26}$$

$$S(x, t) = (t - ax)s_0(x) + (t - ax)^2s_1(x) + (t - ax)^3s_2(x) + \dots \tag{27}$$

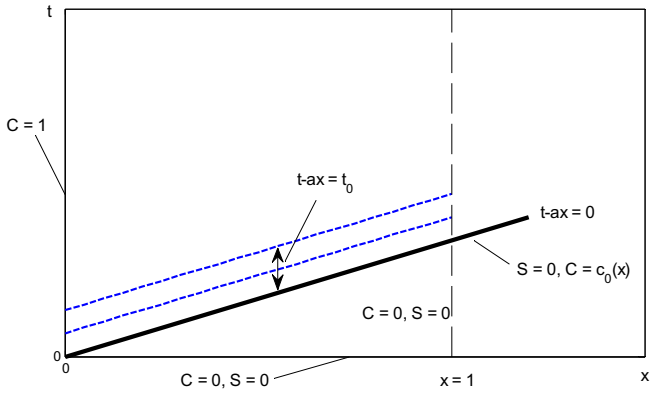

Fig. 2. (x,t) diagram of the flow zone.

The problem is solved in the domain $x > 0, t - ax > 0$. The detailed derivations of zero, first and second order asymptotic systems are presented in Supplementary Information. The solutions derived in Supplementary Information provide the zero, first and second order asymptotic approximations for C and S.

The zero order term $c_0(x), (t-ax)s_0(x)$ is the solution of system (B5)

$$c_0(x) = \left[(af_1 - g_1) + (1 + g_1 - af_1)e^{\frac{\lambda_0}{f_0}x}\right]^{-1} \tag{28}$$

$$s_0(x) = \lambda_0\left[(af_1 - g_1) + (1 + g_1 - af_1)e^{\frac{\lambda_0}{f_0}x}\right]^{-1} \tag{29}$$

and constants $f_0, f_1, \ldots, g_1, g_2, \ldots$ are defined by Eq. (A6).

The first order term has the form $(t-ax)c_1(x), \quad (t-ax)^2 s_1(x)$, determined by system (B6)

$$c_1(x) = \frac{(g_2\lambda_0 - a\lambda_0 f_2) + (1 + g_1 - af_1)\left(\lambda_1 - \frac{2f_1\lambda_0}{f_0}\right)e^{\frac{\lambda_0}{f_0}x} - \left((g_2\lambda_0 - a\lambda_0 f_2) + (1 + g_1 - af_1)\left(\lambda_1 - \frac{2f_1\lambda_0}{f_0}\right)\right)e^{2\frac{\lambda_0}{f_0}x}}{\left((af_1 - g_1) + (1 + g_1 - af_1)e^{\frac{\lambda_0}{f_0}x}\right)^3} \tag{30}$$

$$s_1(x) = \frac{\frac{\lambda_0\lambda_1}{2}(af_1 - g_1) + \lambda_0(1 + g_1 - af_1)\left(\lambda_1 - \frac{f_1\lambda_0}{f_0}\right)e^{\frac{\lambda_0}{f_0}x} - \lambda_0(1 + g_1 - af_1)\left(\frac{\lambda_1}{2} - \frac{f_1\lambda_0}{f_0}\right)e^{2\frac{\lambda_0}{f_0}x}}{\left((af_1 - g_1) + (1 + g_1 - af_1)e^{\frac{\lambda_0}{f_0}x}\right)^3} \tag{31}$$

The second order term $(t-ax)^2 c_2(x), \quad (t-ax)^3 s_2(x)$ is obtained by solving system (B7)

$$c_2(x) = c_0^4(x)e^{3\frac{\lambda_0}{f_0}x}\int_0^x F(x)dx \tag{32}$$

where

$$\begin{aligned} F(x) = \{&3af_1 s_1(x)c_1(x) + 3af_2(x)s_0^2(x)c_1(x) + 6af_2 s_0(x)s_1(x)c_0(x) + 3af_3 s_0^3(x)c_0(x) \\ &-(3g_1 s_1(x)c_1(x) + 3g_2 s_0^2(x)c_1(x) + 6g_2 s_0(x)s_1(x)c_0(x) + 3g_3 s_0^3(x)c_0(x)) \\ &-((g_1 - af_1)c_0(x) + 1)(\lambda_1 s_0(x)c_1(x) + \lambda_1 s_1(x)c_0(x) + \lambda_2 s_0^2(x)c_0(x)) \\ &-[f_1 s_0(x)c_1'(x) + f_1 s_0'(x)c_1(x) + f_1 s_1(x)c_0'(x) + f_1 s_1'(x)c_0(x) \\ &+f_2 s_0^2(x)c_0'(x) + 2f_2 s_0(x)s_0'(x)c_0(x)]\}e^{-3\frac{\lambda_0}{f_0}x}f_0^{-1}c_0^{-4}(x) \end{aligned}$$

and

$$s_2(x) = \frac{1}{3}\left[\lambda_1 s_1(x)c_0(x) + \lambda_2 s_0^2(x)c_0(x) + \lambda_1 s_0(x)c_1(x) + \lambda_0 c_2(x)\right] \tag{33}$$

The zero order approximation

$$\begin{aligned} C_0(x) &= c_0(x) \\ S_0(x,t) &= (t-ax)s_0(x) \end{aligned} \tag{34}$$

is presented in Figs. 8 and 9 by dash-dotted curves, the first order approximation

$$\begin{aligned} C_1(x,t) &= c_0(x) + (t-ax)c_1(x) \\ S_1(x,t) &= (t-ax)s_0(x) + (t-ax)^2 s_1(x) \end{aligned} \tag{35}$$

is given by dashed curves and the second order approximation

$$\begin{aligned} C_2(x,t) &= c_0(x) + (t-ax)c_1(x) + (t-ax)^2 c_2(x) \\ S_2(x,t) &= (t-ax)s_0(x) + (t-ax)^2 s_1(x) + (t-ax)^3 s_2(x) \end{aligned} \tag{36}$$

is shown by solid curves. The solution curves corresponding to the zero, first and second order approximations for three size particles are shown in Fig. 3 for suspended concentration and in Fig. 4 for retained concentration. The difference between the zero and first order approximations highly exceeds the difference between the first and second order approximations. The curves for the first and second order approximations almost coincide for all particle sizes. The deviation between lower and higher order approximations increases with time. However, the difference between the second and first order approximations remains negligible during the overall testing period. Despite more rigorous mathematical analysis is required, the above indicates the convergence of the series (26, 27). Therefore, the second term in asymptotic expansion (32, 33) can be used for the residue estimation. Further in the text, the first order approximation (35) is used as an analytical model to tune the constants in population balance model and the second order approximation (36) is used for estimation of the accuracy of asymptotic modelling.

4. Downscaling expression for expansion terms via micro scale parameters (*H*,*l*)

In this section we present micro scale solutions that correspond to the zero and first order approximations (34, 35).

Substituting the asymptotic solutions (28–31) into (15) and accounting for (16) yields the following downscaling expression for pore concentration distribution:

$$H(r_p, x, t) = H_0(r_p)e^{-k_1 y(h_0 - S_i(x,t)c^0\phi_0 l)} \tag{37}$$

where $i = 0$ and 1 correspond to the zero and first order solutions, respectively. Function $h(y)$ in (37) is obtained by numerical integration in Eq. (16).

The evolution of pore concentration distributions at the core inlet and outlet are presented in Fig. 5(a). There is a delay in pore

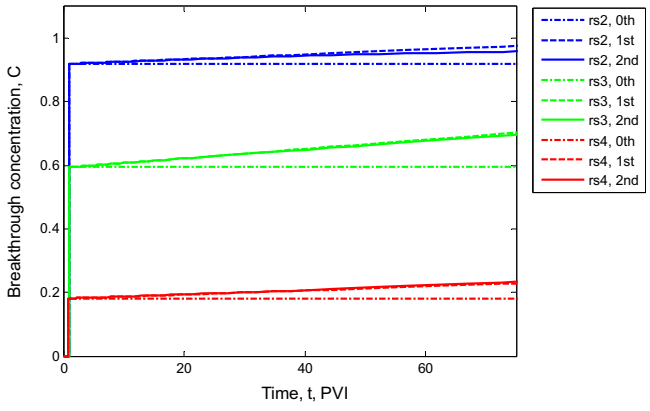

Fig. 3. Breakthrough concentrations obtained from 0th, 1st and 2nd order asymptotic solutions.

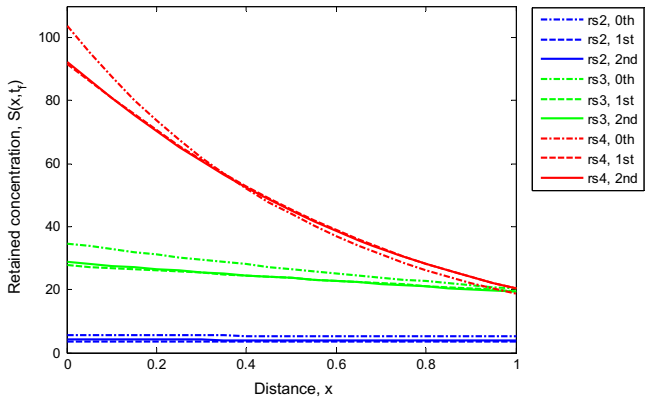

Fig. 4. Retained concentration profiles obtained from 0th, 1st and 2nd order asymptotic solutions.

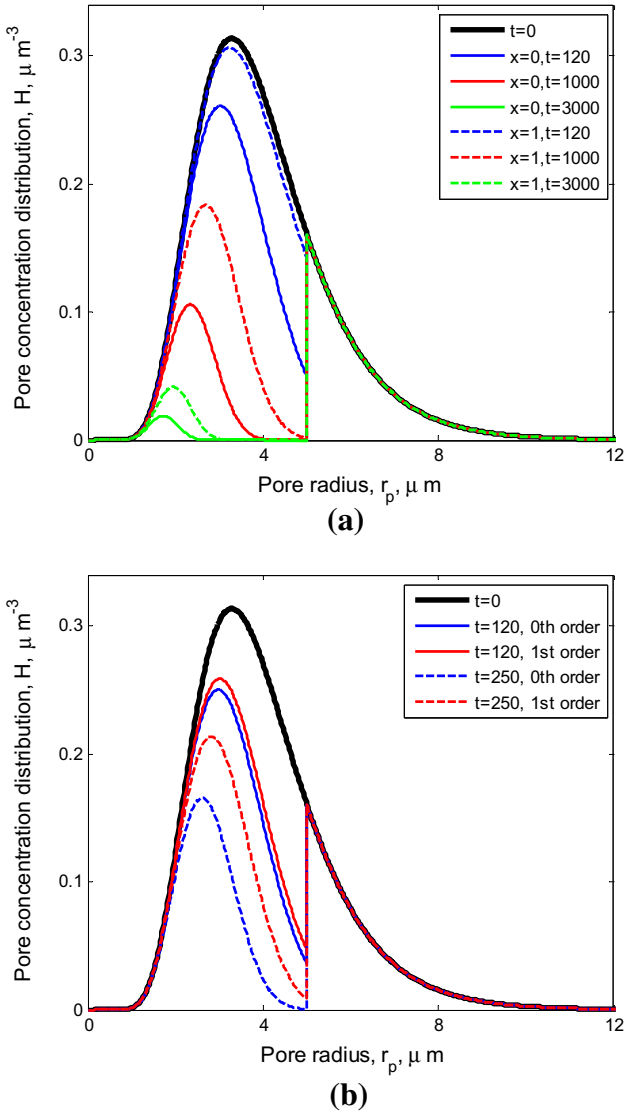

Fig. 5. Evolution of pore concentration distribution at the core inlet (solid curves) and the core outlet (dashed curves): (a) the first order expansion at different moments; (b) comparison between the zero and first order expansions at two moments.

concentration reduction at the outlet if compared with that at the inlet, which is due to particle travel along the overall core.

The wave of disappearing plugged pores propagates from the inlet to the outlet. Concentrations of pores larger than the injected particles do not change with time, since the pores allow particles to pass without being captured. Concentrations of all pores smaller than the particles $r_p < r_0$ decrease with time monotonically. The smaller are the pores the lower is the particle flux through them. Therefore, larger pores are plugged with higher intensity. Pores with size $r_p = r_0$ disappear at the inlet at the moment $t = 1000$ PVI, while they disappear at the outlet at $t = 1500$ PVI. The size interval of the disappeared pores $[r_{pmax}, r_0]$ extends with time. The maximum size of remaining pores tends to zero until the complete plugging of the small pores as time tends to infinity.

Fig. 5(b) shows the results of downscaling for the zero and first order approximations; the corresponding pore size concentration distributions are denoted by continuous and dashed curves, respectively. The first order approximation exhibits faster pore plugging than the zero order approximation. The difference between curves increases with time, which corresponds to Fig. 3 where the deviation between lower and higher order approximations also increases with time.

5. Experimental study of suspension flow in porous media

This section describes the materials used, laboratory setup, experimental procedures and calculations of interaction between the latex particles and porous media. The repulsion conditions are created in order to avoid particle attachment to the grains and pore walls; size exclusion becomes a dominant particle retention mechanism.

5.1. Materials

Spherical soda-lime glass beads with diameters 30–50 μm (Catalog Number 18901, Polysciences, Inc., Warrington, PA, USA) are used for the preparation of an engineered porous medium. The glass beads have the following chemical composition (% by weight): SiO_2 – 66–75, Al_2O_3 – 0–5, CaO – 6–15, MgO – 1–5, Na_2O – 10–20, and Fe_2O_3 – <0.8. Organic impurities are removed from the surface of glass beads by washing in the following sequence with hexane, acetone, MilliQ water, hydrochloric acid and MilliQ water. The beads are wet-packed into the flow-through column in order to eliminate ingress of air pockets and achieve a homogeneity of the porous medium.

Fluorescent yellow-green latex microspheres modified with surface carboxyl groups (Polysciences, Inc., Warrington, PA, USA) are used for suspension preparation. The mono-sized particles with the following radii are used in each test: $r_{s1} = 1.568$, $r_{s2} = 2.179$ and $r_{s3} = 3.168$ μm, which further in the text are called the first, second and third particle radii, respectively. Particles with the smallest radius $r_{s0} = 0.510$ μm have also been injected. Concentrations of the injected latex particle suspensions vary from 1 to 4 ppm.

The suspensions are prepared using deionised high-purity MilliQ water (EMD Millipore, former Millipore Corporation, USA) with electrical resistivity of 18.2 MOhm × cm at 25 °C. Carboxyl groups undergo deprotonation resulting in a negative net surface charge for latex particles. Glass beads also develop a negative net surface charge in alkaline solutions. It promotes the repulsion between the latex particles and glass beads leading to a dominant size exclusion mechanism for the particle capture. To guarantee the repulsion conditions, the suspension alkalinity at pH above 10 is adjusted by addition of an aqueous NaOH solution to the MilliQ water.

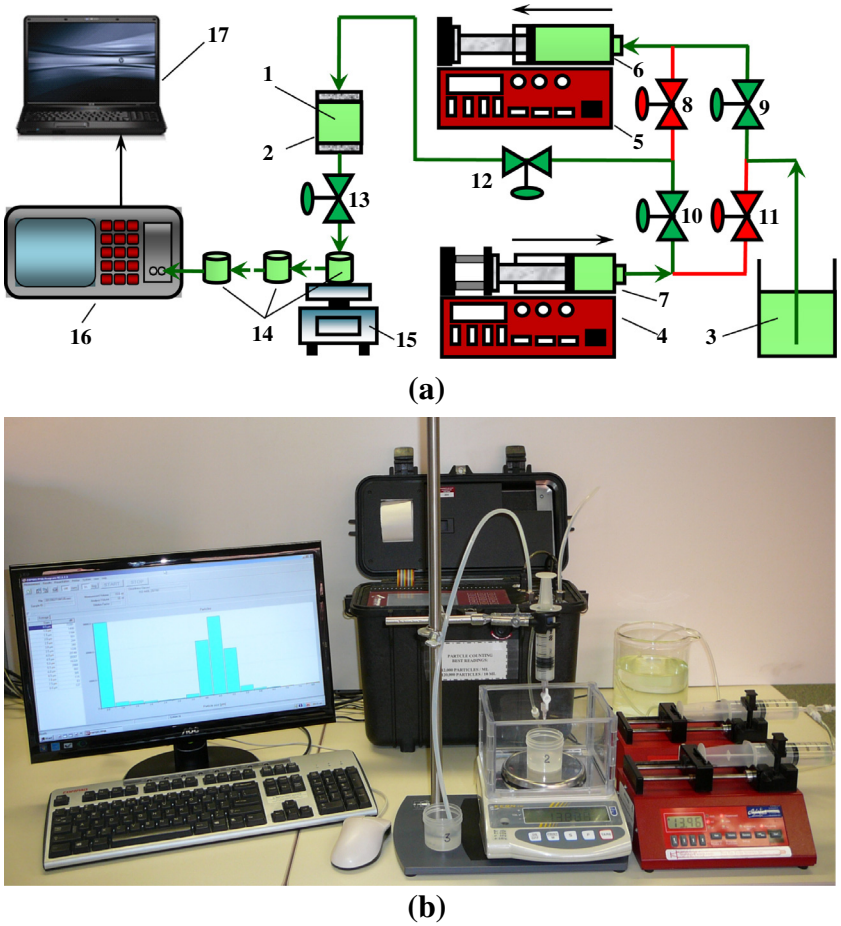

Fig. 6. (a) Schematic of laboratory setup; (b) Photo of laboratory setup: 1 – glass beads; 2 – flow-through column; 3 – suspension with latex microspheres; 4, 5 – syringe pumps; 6, 7 – syringes; 8–11 – one-way valves; 12, 13 – manual valves; 14 – collecting beakers; 15 – analytical balance; 16 – PAMAS particle counter; 17 – stand-alone computer.

5.2. Experimental setup and procedures

Laboratory setup used in the present study is schematically shown in Fig. 6 and is described in details in [40]. Two pulseless syringe pumps (NE-1000 dual syringe pumps 1 and 2, New Era Pump Systems, Inc., Farmingdale, NY, USA) uninterruptedly deliver suspension with latex particles top-to-bottom in the flow-through column. The effluent sample masses are measured by an analytical balance (KERN EW 420-3NM, Inscale Ltd., Bucks, UK). Particle counter PAMAS S4031 GO (PAMAS GmbH, Salzuflen, Germany, referred further in the text as PAMAS) measures the number and size distribution of latex particles which are converted in ppm. The following data characterise: packed column The length and diameter of the flow-through column packed with glass beads are equal to 1.594 and 2.336 cm, respectively. The porosity for the rhombohedral packing of spherical glass beads is assumed to be equal to 0.396 (see the monograph by Dullien [41]). The pore volume is equal to 2.705 cm^3.

The normalised retained particle concentration along the flow-through column is determined after the completion of the size exclusion experiments. The compacted glass beads with retained latex particles are removed from the column and are split in three parts of about 0.5 cm in length. Mass of each sample is measured by an analytical balance. Each sample is placed in a separate beaker. MilliQ water with pH adjusted at above 10 is added to the beaker at the ratio of 40 mL/g. Ultrasonification of these glass beads results in release of the retained latex particles. The particles are released into suspensions; their concentration is measured by PAMAS.

5.3. Electrophoretic mobility, surface and zeta potentials, and interaction energy

The total potential energy of interaction between latex microspheres and glass beads is calculated by Derjaguin–Landau–Verwey–Overbeek (DLVO) theory [42,43]. Potential energy of interaction is calculated using the values of zeta potentials for latex particles and glass beads which in turn are calculated using the respective experimental electrophoretic mobility data. The electrophoretic mobilities for latex microspheres and glass beads are measured by Zetasizer Nano ZS (Malvern Instruments Ltd., Worcestershire, UK).

Electrophoretic mobility of solid micro-sized particles in suspensions with high ionic strength vanishes. However, there does exist a residual non-zero electrophoretic mobility of -1.268×10^{-8} $m^2/(V\times s)$ for carboxyl-modified latex particles in MilliQ water-based suspensions with ionic strength of 1 M NaCl (see Badalyan et al. [40]). Therefore, the carboxyl modified latex particles should be considered as the so-called "soft" particles [44]. The "softness" causes the penetration of ions from an electrolyte solution into the polyelectrolyte (carboxyl) layer. The ion penetration distorts the electrical double layer surrounding latex particle and changes the particle surface charge.

The outer surface potential for carboxyl-modified latex particles is calculated using the Ohshima theory for "soft" particles [45,46] for the electrophoretic mobility data that correspond to the present experimental conditions (ionic strength of 6.24×10^{-5} M and pH at about 10, see [40]): $\psi_s = -206.8$ mV. Zeta potential for glass beads at the present experimental conditions is calculated according to the Henry's expression (see [47]) accounting for electrophoretic retardation and relaxation effects: $\zeta_b = -51.99$ mV. The outer surface potential for latex particles and zeta potential for glass beads are used for calculation of the repulsive electric double-layer interaction potential energy (EDL).

The total potential energy of interactions between the latex particles and glass beads is equal to the sum of those from the attractive long-range London-van der Waals (LW), the short-range repulsive EDL and Born forces. Equations proposed by Gregory [48,49] are used for calculation of LW and repulsive EDL potential energies of interactions, and Born interaction energy is calculated according to the equation introduced by Ruckenstein and Prieve [50].

Variation of the DLVO total interaction potential energy as a function of the separation distance between latex microspheres and glass beads is calculated for latex particles with radius of 3.168 μm and presented in Fig. 7. A very high repulsive potential energy barrier of 63,620 k_BT indicates that latex particles having an average energy of Brownian motion of about 1.5 k_BT are unable to overcome this barrier and be trapped in the primary energy minimum. Besides, the primary energy minimum has very high positive value of 62,573 k_BT at separation distance of 0.33 nm meaning that latex particles cannot approach the surface of glass beads due to mutual repulsion.

A shallow negative secondary minimum of -0.056 k_BT at the separation distance of about 436 nm may indicate to the possibility for latex particles to be reversibly trapped in this minimum and attached to the surface of glass beads (see insert in Fig. 7). However, the average energy of Brownian motion for latex particles is high enough to overcome the attraction from glass beads, and the particles can escape without being attached to glass beads.

Finally, the latex particles cannot be electrostatically attached to glass beads for the entire range of separation distance under the conditions of the performed tests. Therefore, the dominant particle retention mechanism in the present study is size exclusion particle capture.

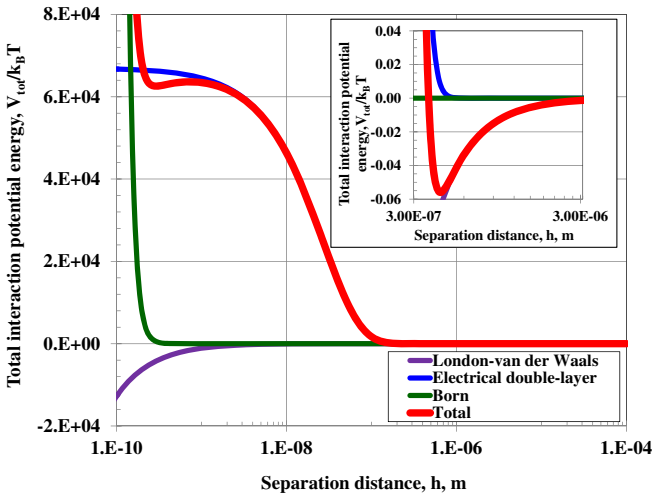

Fig. 7. Total potential energy of interaction between latex particles and glass beads with zoom near to the secondary potential energy minimum.

6. Laboratory data treatment by the asymptotic model

In this section, history matching of the suspension flow test data with two particle sizes by the asymptotic model is performed, and the prediction by the tuned model is compared with the experimental data for the third particle size (subsection 6.1). The laboratory measurements uncertainties, deviation between the modelling and experimental data and the asymptotic modelling accuracy are introduced in subsections 6.2, 6.3 and 6.4, respectively. The comparison between the above three values for conditions of the laboratory study and asymptotic modelling results in the conclusion about the validity of asymptotic method for the laboratory-based predictive modelling (subsection 6.5).

6.1. History matching of experimental data and predictive modelling

Four mono-sized coreflood tests of different particle sizes have been performed. The measured breakthrough concentrations of particles with the first and second radii are used for the model tuning in order to determine the model parameters – mean and variance coefficient for two-parametric pore throat size distribution, maximum inter-chamber distance and its exponent – from the breakthrough concentrations of particles with the first and second radii. The deviation of the breakthrough concentration from the smallest particles from unity is significantly lower than the accuracy of measurements, so these data does not contribute to the model tuning. The third radius particle test is used for comparison with the model prediction.

It is assumed that the initial pore size distribution of the engineered porous medium fulfils the conditions of the breakage algorithm and, therefore, is lognormal (see [51] for details). Therefore, the distribution is defined by the mean pore radius $\langle r_p \rangle$ and variance coefficient C_v. The inter-chamber distance is the power-law function of the fractional flow defined by the constant value l_0 and the power β, see (10). The population balance model becomes four-parametric under the above assumptions.

Least squares goal function of deviation between the model predicted and measured data is used in the model tuning procedure. The Levenburg-Marquardt minimization algorithm has been applied [52]. The optimised model constants are: $\langle r_p \rangle = 3.44$ μm, $C_v = 0.31$, $l_0 = 0.21$ μm and $\beta = 0.58$. Good match of the breakthrough curves by the model is shown in Fig. 8. The coefficient of determination for the curves with the first and second particle radii are $R^2 = 0.995$ and 0.993, respectively.

The history matching based model tuning allows for data prediction and their comparison with other experimental results. The measured and the tuned-model-predicted curves for the third

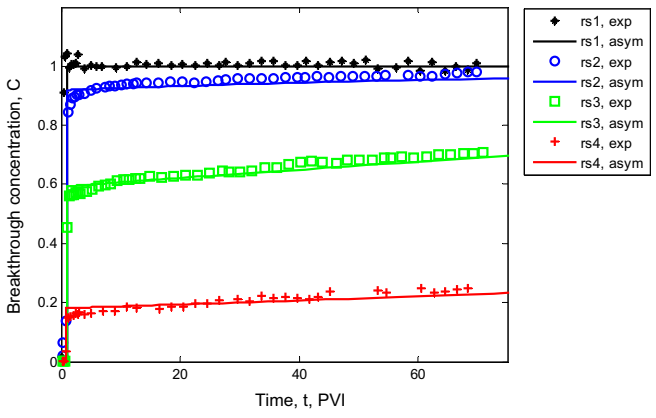

Fig. 8. Breakthrough concentration versus time: model tuning ($r_{s1} \sim r_{s3}$) and prediction (r_{s4}).

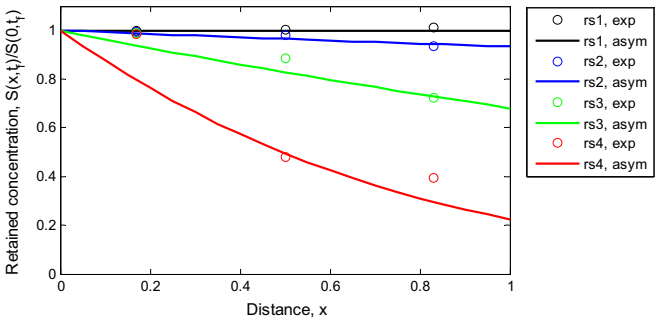

Fig. 9. Comparison of retained concentration profiles between experimental data and the asymptotic solution.

radius particles are in good agreement, indicated by the coefficient of determination $R^2 = 0.975$ (Fig. 8).

Fig. 9 presents the retained profiles for particles with four radii obtained from the tuned asymptotic model. The retained concentrations have been measured post-mortem by dividing the core into three pieces and weighting. So, the averaged concentrations in three intervals have been determined from the asymptotic model and compared with the measured data. The coefficients of determination for three particle radii are $R^2 = 0.963$, 0.950 and 0.899, respectively.

6.2. Uncertainties in laboratory measurements

The accuracy of laboratory measurement is estimated by the combined standard uncertainties (CSU) using the linear uncertainty propagation method [53]:

$$u(z) = \sqrt{\sum_{i=1}^{N}\left[\left(\frac{\partial f}{\partial y_i}\right)u(y_i)\right]^2} \tag{38}$$

where $u(z)$ is the combined standard uncertainties of the function $z = f(y_1, \ldots y_i \ldots y_N)$; $u(y_i)$ is standard uncertainty associated with the input parameter y_i; $\partial f/\partial y_i$ is sensitivity coefficient; i is the number of the input parameter; N is the total number of the input parameters.

For the measurement of effluent concentration, there are two input parameters in (38): $y_1 = C^L$, $y_2 = C^0$ (see [40] for details). The function f is equal to y_1/y_2. $u(C^L)$ and $u(C^0)$ are the combined standard uncertainties for inlet and outlet suspension concentrations, respectively. The relative combined standard uncertainties δ_C is calculated from $u(C^L/C^0)/C^0$ and presented in the third column of Table 1.

For the retained concentration measurement, define the four input parameters in (38) as $y_1 = V_{wk}$, $y_2 = c_{\sigma k}$, $y_3 = c^0$ and $y_4 = M_k$. The results of relative uncertainty δ_S are shown in the fifth column of Table 1.

6.3. Deviation between the modelling and laboratory data

The normalised least square deviation of the model (first order asymptotic solution) from the measured data is calculated as:

$$E_C = \sqrt{\frac{1}{t_f}\int_0^{t_f}\left[\frac{C_1(1,t) - C_{\exp}(1,t)}{C_{\exp}(1,t)}\right]^2 dt}$$
$$E_S = \sqrt{\int_0^1\left[\frac{S_1(x,t_f) - S_{\exp}(x,t_f)}{S_{\exp}(x,t_f)}\right]^2 dx} \tag{39}$$

for suspended and retained concentrations respectively. The results for three particle sizes are presented in second column of Table 1 for suspended concentration and in fourth column for retained concentration.

6.4. Accuracy of the asymptotic model

Let us define the accuracy of the first order asymptotic expansion (35) consistent with the above introduced relative combined standard uncertainty and the deviations (39). The second order approximation evaluates the exact model prediction while the residue is represented by the second order asymptotic term. The following expressions

$$D_{C12} = \sqrt{\frac{1}{t_f}\int_0^{t_f}\left[\frac{C_2(1,t) - C_1(1,t)}{C_2(1,t)}\right]^2 dt}$$
$$D_{S12} = \sqrt{\int_0^1\left[\frac{S_2(x,t_f) - S_1(x,t_f)}{S_2(x,t_f)}\right]^2 dx} \tag{40}$$

where t_f is the total injection time in the test, are the normalised least square residues of the first order approximation.

The accuracies of the zero order approximations D_{C01} and D_{S01} are defined from the first order term of the expansion similarly to (40). The results are presented in Table 2.

6.5. Analysis of the data accuracy and uncertainty

Three criteria introduced above for accuracy of laboratory measurements, of the first order asymptotic model and the normalised deviation between the laboratory and modelling data have the form of the variance coefficient, which is the ratio between the standard deviation and the mean value. The criteria are consistent with each other and used below for validation of the first order asymptotic model.

The normalised least square residues for the first order asymptotic model are shown in second and fourth columns of Table 2; third and fifth columns show normalised least square residues for the zero order approximation. The residues for the first order asymptotic model are significantly lower than those for the zero order approximation for both suspended and retained concentrations for all size particles, which indicates the convergence of the series.

Tables 1 and 2 show that the variance coefficient D_{C12} of the first order asymptotic solution, which is the model used for tuning of the breakthrough concentration, is significantly lower than the relative combined standard uncertainties for measurements of the breakthrough concentration, $D_{C12} \ll \delta_C$. Therefore, the accuracy of the asymptotic model does not contribute significantly to the matching error.

Table 2 shows that the normalised deviations for breakthrough concentrations of the first and second particle radii is smaller than

Table 1
Accuracy analysis from the asymptotic solution and experimental data.

r_s (μm)	E_C (%)	δ_C (%)	E_S (%)	δ_S (%)	$t_{l,1}$	$t_{l,0}$
1.568	1.79	2.29	2.25	2.96	87.56	30.34
2.179	1.56	1.81	3.49	2.84	119.77	9.46
3.168	0.89	2.48	5.72	5.53	82.90	9.60

Table 2
Accuracy analysis of the asymptotic solution.

r_s (μm)	D_{C12} (%)	D_{C02} (%)	D_{S12} (%)	D_{S02} (%)
1.568	0.23	0.92	6.47	24.98
2.179	0.11	2.97	1.48	13.49
3.168	0.27	4.27	0.44	6.42

the corresponding relative combined standard uncertainties, which indicates good match of breakthrough concentrations by the asymptotic model. The fourth row of the Table 2 exhibits same inequality for breakthrough concentrations of the third radius particles, so the quality of the breakthrough concentration prediction is also good. Although the required inequality $E_S < \delta_S$ for the normalised deviation and the relative combined standard uncertainties for retained concentration do not hold for the second and third radii, the values are close to each other. It allows claiming qualitative agreement between the experimental data on the retained concentration profiles and the data of predictive modelling.

Let us determine time interval where the first order asymptotic model is valid. The second asymptotic term provides the estimate for the residue. The first order model can be applied where the normalised residue does not exceed the accuracy of measurements, i.e. the valid period of the first order solution $t_{l,1}$ is determined from the equality

$$\frac{|C_2(1,t_{l,1}) - C_1(1,t_{l,1})|}{C_2(1,t_{l,1})} = \delta_C \tag{41}$$

The validity period values are presented in sixth column of the Table 1. The values exceed 70 PVI applied in the presented study, confirming the validity of the model during the test time period.

The valid period for the zero order solution $t_{l,0}$ is determined as

$$\frac{|C_1(1,t_{l,0}) - C_0(1,t_{l,0})|}{C_2(1,t_{l,0})} = \delta_C \tag{42}$$

The time period for the validity of the first order asymptotic model $t_{l,1}$ is significantly longer than that of the zero order approximation model $t_{l,0}$, allowing using significantly larger amount of information for the model adjustment and tuning of the model constants.

7. Discussions

Each term of the asymptotic expansions for the initial and boundary conditions (24, 25) provide with unique solution for each term of the expansion for system (34–36) up to the second order. The rigorous analysis requires checking these conditions for all terms with proof of the convergence. However, for the purposes of current work the claim of the regular expansion is limited by the analysis of the zero, first and second approximations only.

Treatment of breakthrough curves using the linearised model (3) provides with only one constant per particle size; the constant is determined by the effluent concentration at the breakthrough moment. Moreover, unknown time interval where the breakthrough concentration is constant decreases the accuracy of its measurement. Breakthrough concentration increases with time, which increases degree of freedom of the treated information by one in the case of linear breakthrough curves and at least by two for non-linear growth. For a given number of coreflood by different radii particles, treatment of the long-term breakthrough curves by the asymptotic model increases the accuracy of the model tuning. Very limited number of different particle sizes is available in the market. Using the asymptotic model for the parameter tuning, yields the decrease in the necessary number of different particle sizes.

For example, three different size particles have been used for mono-sized suspension coreflood in the presented laboratory study. Lognormal pore throat size distribution was assumed. The population balance model has four degrees of freedom: two constants determine the lognormal size distribution and two constants determine the correlation length function of the particle radius. So, three constant breakthrough concentrations does not allow for the model adjustment. Application of the asymptotic model allows for the history matching from two tests, leaving the third test for the model validation.

Two tuned breakthrough concentration histories exhibit good quality of history matching, which validates the asymptotic model. Good agreement between the experimental data and fully predictive modelling for the third test also validates the model. However, only qualitative agreement between the measured effluent concentration history and that fully predicted by modelling has been observed. It is explained by low accuracy of the retention profile measurements. More accurate measurements such as CT scanning in the future tests would allow further validation of the model [2,3].

The asymptotic solution allows determining the time interval where the model is valid. It also allows determining the validity time for the constant breakthrough concentration, improving the routine procedure.

The presented study aims the prolongation of the after-the-breakthrough period where an analytical model can treat the breakthrough concentration. So, this period $(t - ax)$ is chosen as a small parameter, i.e., the solution is expanded behind the breakthrough front. Another way of the asymptotic integration could be the choice of the maximum retained concentration as a small parameter. The method can be applied not only for the upscaled system (22, 23), but also for the population balance model with distributed particle and pore sizes (7–9).

We discuss the general case of particle capture due to size exclusion, electrostatic attachment, segregation, diffusion into dead end pores, etc. The filtration coefficient is presented in Eqs. (8) and (9) as the sum of pure size-exclusion term and all other mechanisms by introduction of the particle capture probability "inside" the pore. However, the laboratory tests are designed to tune the model from two injections with two different particle sizes, so the simplified conditions of size exclusion domination have been created during laboratory tests. Adjustment of the model with both straining and attachment can be performed using the asymptotic model (28–33) but requires the larger number of tests.

The first order asymptotic solution allows adjusting the mathematical model based on the breakthrough concentration during the time significantly longer than the period where the solution of the linearised model is valid. Involvement of the larger amount of information for tuning yields fewer tests and, consequently, smaller number of different size particles. The comparison between the zero, first and second order terms indicates convergence of asymptotic expansion, allowing using the last expansion term for the residue estimate. The period where the first order approximation is valid is estimated from the second order approximation and is found to vary between 82.90 and 119.77 PVI for the laboratory conditions performed. The valid period of the zero order approximation is obtained from the first order approximation and varies from 9.46 to 30.34 PVI. So, the first order approximation is valid during significantly larger period than the zero order solution (3).

8. Conclusions

Asymptotic integration of non-linear deep bed filtration model along with laboratory study allows drawing the following conclusions:

(1) One-dimensional large-scale system of deep bed filtration allows for asymptotic expansion behind the concentration front with explicit formulae for second order approximation.
(2) Since the large scale system is obtained from the small-scale population balance model by exact averaging, the asymptotic solution obtained allows for downscaling, describing timely evolution of pore size distribution due to pore plugging during the mono-sized suspension injection.

(3) Downscaling of the first order asymptotic solution shows that the intermediate size pores smaller than the injected particles are plugged faster than small pores, resulting in earlier disappearance of the intermediate size pores. The pores with radius equal to the injected particle radius disappear first.
(4) The first order asymptotic model allows for history matching during significantly larger time interval than that by the linearised model.
(5) The validity time of the linear-model-based estimates is obtained from the first order asymptotic model.
(6) Good match between the laboratory and modelling suspension concentrations has been observed during the tuning of the population balance model from two injections of mono-sized particles.
(7) Good agreement between the laboratory data on suspended concentration of the third size particles and the prediction by the tuned model is observed.
(8) Using the asymptotic solution improves the quality of tuning for the population balance model, requiring fewer mono-sized suspension injections.

Acknowledgements

Authors are grateful to Dr Alexander Badalyan (Australian School of Petroleum, the University of Adelaide) for calculation of electrostatic forces, design of the laboratory set-up and development of the test methodology. Authors thank Dr Mohammad Sayyafzadeh (Australian School of Petroleum, the University of Adelaide) for fruitful discussions of uncertainty and accuracy. Eng. Kaiser Aji is acknowledged for running the tests. The work was sponsored by grants DP1094299, LP100100613 and LP110200799 of the Australian Research Council.

Appendix A. Supplementary data

Supplementary data associated with this article can be found, in the online version, at http://dx.doi.org/10.1016/j.cej.2014.07.051.

References

[1] P. Bedrikovetsky, Mathematical theory of oil and gas recovery: with applications to ex-USSR oil and gas fields, Kluwer Academic, Dordrecht, 1993.
[2] D.C. Mays, J.R. Hunt, Hydrodynamic aspects of particle clogging in porous media, Environ. Sci. Technol. 39 (2005) 577–584.
[3] D.C. Mays, J.R. Hunt, Hydrodynamic and chemical factors in clogging by montmorillonite in porous media, Environ. Sci. Technol. 41 (2007) 5666–5671.
[4] F. Civan, Reservoir formation damage: fundamentals, modeling, assessment, and mitigation, second ed., Gulf Publishing Company, Houston, Texas, 2007.
[5] N. Tufenkji, Colloid and microbe migration in granular environments: A discussion of modelling methods, in: F.H. Frimmel, F. von der Kammer, H.-C. Flemming (Eds.), Colloidal Transport in Porous Media, Springer, Berlin, Germany, 2007, pp. 119–142.
[6] S. Torkzaban, S.A. Bradford, S.L. Walker, Resolving the coupled effects of hydrodynamics and DLVO forces on colloid attachment in porous media, Langmuir 23 (2007) 9652–9660.
[7] V. Gitis, I. Rubinstein, M. Livshits, G. Ziskind, Deep-bed filtration model with multistage deposition kinetics, Chem. Eng. J. 163 (2010) 78–85.
[8] C. Noubactep, S. Caré, Dimensioning metallic iron beds for efficient contaminant removal, Chem. Eng. J. 163 (2010) 454–460.
[9] V. Gitis, C. Dlugy, G. Ziskind, S. Sladkevich, O. Lev, Fluorescent clays — similar transfer with sensitive detection, Chem. Eng. J. 174 (2011) 482–488.
[10] H. Yuan, A.A. Shapiro, A mathematical model for non-monotonic deposition profiles in deep bed filtration systems, Chem. Eng. J. 166 (2011) 105–115.
[11] H. Yuan, A.A. Shapiro, Z. You, A. Badalyan, Estimating filtration coefficients for straining from percolation and random walk theories, Chem. Eng. J. 210 (2012) 63–73.
[12] J.P. Herzig, D.M. Leclerc, P. Legoff, Flow of suspensions through porous media – application to deep filtration, Ind. Eng. Chem. 62 (1970) 8–35.
[13] M. Elimelech, X. Jia, J. Gregory, R. Williams, Particle Deposition and Aggregation: Measurement, Modelling and Simulation, Butterworth-Heinemann, Oxford, 1998.
[14] S.A. Bradford, S. Torkzaban, Colloid transport and retention in unsaturated porous media: a review of interface-, collector-, and pore-scale processes and models, Vadose Zone J. 7 (2008) 667–681.
[15] S. Sirivithayapakorn, A. Keller, Transport of colloids in saturated porous media: a pore-scale observation of the size exclusion effect and colloid acceleration, Water Resour. Res. 39 (2003) SBH111–SBH1111.
[16] A. Santos, P. Bedrikovetsky, A stochastic model for particulate suspension flow in porous media, Transp. Porous Media 62 (2006) 23–53.
[17] M.T. van Genuchten, W.J. Alves, Analytical solutions of the one-dimensional convective–dispersive solute transport equation, U.S. Dept. of Agriculture, Agricultural Research Service, Washington, D.C., 1982.
[18] G. Ziskind, H. Shmueli, V. Gitis, An analytical solution of the convection–dispersion-reaction equation for a finite region with a pulse boundary condition, Chem. Eng. J. 167 (2011) 403–408.
[19] J.S. Pérez Guerrero, L.C.G. Pimentel, T.H. Skaggs, M.T. Van Genuchten, Analytical solution of the advection–diffusion transport equation using a change-of-variable and integral transform technique, Int. J. Heat Mass Transf. 52 (2009) 3297–3304.
[20] J.S. Pérez Guerrero, E.M. Pontedeiro, M.T. van Genuchten, T.H. Skaggs, Analytical solutions of the one-dimensional advection–dispersion solute transport equation subject to time-dependent boundary conditions, Chem. Eng. J. 221 (2013) 487–491.
[21] M.M. Sharma, Y.C. Yortsos, Transport of particulate suspensions in porous media: model formulation, AIChE J. 33 (1987) 1636–1643.
[22] M.M. Sharma, Y.C. Yortsos, Network model for deep bed filtration processes, AIChE J. 33 (1987) 1644–1653.
[23] M.M. Sharma, Y.C. Yortsos, Fines migration in porous media, AIChE J. 33 (1987) 1654–1662.
[24] P. Bedrikovetsky, Upscaling of stochastic micro model for suspension transport in porous media, Transp. Porous Media 75 (2008) 335–369.
[25] A.C. Payatakes, C. Tien, R.M. Turian, A new model for granular porous media: Part I. Model formulation, AIChE J. 19 (1973) 58–67.
[26] A.C. Payatakes, R. Rajagopalan, C. Tien, Application of porous media models to the study of deep bed filtration, Can. J. Chem. Eng. 52 (1974) 722–731.
[27] A. Cortis, B. Berkowitz, Anomalous transport in "classical" soil and sand columns, Soil Sci. Soc. Am. J. 68 (2004) 1539–1548.
[28] A. Cortis, T. Harter, L. Hou, E.R. Atwill, A.I. Packman, P.G. Green, Transport of *Cryptosporidium parvum* in porous media: long-term elution experiments and continuous time random walk filtration modeling, Water Resour. Res. 42 (2006) W12S13.
[29] A.A. Shapiro, Elliptic equation for random walks. Application to transport in microporous media, Physica A 375 (2007) 81–96.
[30] H.K. Lin, L.P. Pryadko, S. Walker, R. Zandi, Attachment and detachment rate distributions in deep-bed filtration, Phys. Rev. E Stat. Nonlinear Soft Matter Phys. 79 (2009) 046321.
[31] H. Yuan, A.A. Shapiro, Modeling non-Fickian transport and hyperexponential deposition for deep bed filtration, Chem. Eng. J. 162 (2010) 974–988.
[32] H. Yuan, G. Sin, Uncertainty and sensitivity analysis of filtration models for non-Fickian transport and hyperexponential deposition, Chem. Eng. J. 168 (2011) 635–648.
[33] S.A. Bradford, H.N. Kim, B.Z. Haznedaroglu, S. Torkzaban, S.L. Walker, Coupled factors influencing concentration-dependent colloid transport and retention in saturated porous media, Environ. Sci. Technol. 43 (2009) 6996–7002.
[34] A.C. Alvarez, P.G. Bedrikovetsky, G. Hime, A.O. Marchesin, D. Marchesin, J.R. Rodrigues, A fast inverse solver for the filtration function for flow of water with particles in porous media, Inverse Prob. 22 (2006) 69–88.
[35] A.C. Alvarez, G. Hime, D. Marchesin, P.G. Bedrikovetsky, The inverse problem of determining the filtration function and permeability reduction in flow of water with particles in porous media, Transp. Porous Media 70 (2007) 43–62.
[36] S.A. Bradford, S. Torkzaban, J. Simunek, Modeling colloid transport and retention in saturated porous media under unfavorable attachment conditions, Water Resour. Res. 47 (2011) W10503.
[37] P. Chalk, N. Gooding, S. Hutten, Z. You, P. Bedrikovetsky, Pore size distribution from challenge coreflood testing by colloidal flow, Chem. Eng. Res. Des. 90 (2012) 63–77.
[38] H. Yuan, Z. You, A.A. Shapiro, P. Bedrikovetsky, Improved population balance model for straining-dominant deep bed filtration using network calculations, Chem. Eng. J. 226 (2013) 227–237.
[39] R. Courant, D. Hilbert, Methods of Mathematical Physics, Interscience Publishers, New York, 1962.
[40] A. Badalyan, Z. You, K. Aji, P. Bedrikovetsky, T. Carageorgos, A. Zeinijahromi, Size exclusion deep bed filtration: experimental and modelling uncertainties, Rev. Sci. Instrum. 85 (2014). art. No.: 015111.
[41] F.A.L. Dullien, Porous Media: Fluid Transport and Pore Structure, second ed., Academic press Inc., San Diego, CA, 1992.
[42] B. Derjaguin, L. Landau, Theory of the stability of strongly charged lyophobic sols and of the adhesion of strongly charged particles in solutions of electrolytes, Prog. Surf. Sci. 43 (1993) 30–59.
[43] E.J.W. Verwey, J.T.G. Overbeek, Theory of the Stability of Lyophobic Colloids, General Publishing Company, Toronto, Canada, 1999.
[44] Z.A. Kuznar, M. Elimelech, Direct microscopic observation of particle deposition in porous media: role of the secondary energy minimum, Colloids Surf., A 294 (2007) 156–162.
[45] H. Ohshima, Electrophoretic mobility of soft particles, J. Colloid Interface Sci. 163 (1994) 474–483.

[46] H. Ohshima, Theory of electrostatics and electrokinetics of soft particles, Sci. Technol. Adv. Mater. 10 (2009) 063001.
[47] R.J. Hunter, Zeta Potential in Colloid Science: Principles and Applications, Academic Press, Sydney, 1981.
[48] J. Gregory, Interaction of unequal double layers at constant charge, J. Colloid Interface Sci. 51 (1975) 44–51.
[49] J. Gregory, Approximate expressions for retarded van der Waals interactions, J. Colloid Interface Sci. 83 (1981) 138–145.
[50] E. Ruckenstein, D.C. Prieve, Adsorption and desorption of particles and their chromatographic separation, Am. Inst. Chem. Eng. J. 22 (1976) 276–283.
[51] J.L. Jensen, Statistics for Petroleum Engineers and Geoscientists, second ed., Elsevier, Amsterdam, 2000.
[52] D. Marquardt, An algorithm for least-squares estimation of nonlinear parameters, J. Soc. Ind. Appl. Math. 11 (1963) 431–441.
[53] B.N. Taylor, C.E. Kuyatt, Guidelines for Evaluating and Expressing the Uncertainty of NIST Measurement Results, National Institute of Standards and Technology Technical Note 1297, U.S. Government Printing Office, Washington, D.C., 1994.